Advanced Nonlinear Control of Grid Forming Battery Energy Storage Inverters for Enhanced Transient and Voltage Stability: Application to the Nigeria 330 kV Transmission Network

Muibi K. A.[1*]; Johnson T.[2]; Ogundero I. O.[3]; Jimoh E. G.[4]

[1,3,4]Department of Electrical and Electronics Engineering, School of Engineering, Yaba College of Technology, Yaba, Lagos State, Nigeria
[2]Department of Physical Science, School of Science, Yaba College of Technology, Yaba, Lagos State, Nigeria

Corresponding Author: Muibi K. A.[1*]

Publication Date: 2026/09/19

Abstract: The 330 kV national transmission network of Nigeria is a 34-bus, 38-line and 14-generator system. The network suffers endemic voltage instability and transient fragility due to the increasing replacement of synchronous generation by inverter-based resources (IBRs). Power flow studies performed in the Power System Analysis Toolbox (PSAT) show undervoltage violations at Gombe (0.9068 p.u.) and Jos (0.9489 p.u.) busses, a negative reduced Jacobian eigenvalue (0.464) indicating small signal instability, a maximum loadability parameter of λ_critical = 1.7337, and unbounded rotor angle divergence for three phase short circuit contingencies. We develop a hierarchical nonlinear control methodology for grid forming (GFM) inverters with battery energy storage systems (BESS), comprising (i) a Lyapunov stable adaptive virtual synchronous machine (VSM) with a dynamically modulated virtual inertia J and damping D, (ii) a finite horizon model predictive control (MPC) voltage loop co-optimizing voltage tracking, dq axis current limiting, and state of charge (SoC) preservation, and (iii) a washout filtered transient damping injection channel. The Nigerian 330 kV network data parameterized switching level MATLAB/Simulink simulations show 38.6% improvement in the frequency nadir, 45.5% faster postfault voltage recovery, 1.15 p.u. peak inverter current and voltage unbalance factor below the IEC 2% grid code limit under asymmetrical faults, addressing documented Nigerian grid failure modes.

Keywords: *Adaptive Virtual Synchronous Machine; Grid Forming Inverter; Model Predictive Control; Transient Stability; Voltage Recovery.*

How to Cite: Muibi K. A.; Johnson T.; Ogundero I. O.; Jimoh E. G. (2026) Advanced Nonlinear Control of Grid Forming Battery Energy Storage Inverters for Enhanced Transient and Voltage Stability: Application to the Nigeria 330 kV Transmission Network. *International Journal of Innovative Science and Research Technology,* 11(9), 451-462. https://doi.org/10.38124/ijisrt/26sep124

I. INTRODUCTION

The worldwide energy revolution has quickened the displacement of synchronous generators by IBRs, eroding inertia, damping and reactive power reserves, which are critical for power system stability [1]. This deterioration is painfully pronounced in structurally weak grids of developing nations when generating sufficiency, network redundancy and reactive compensating architecture are all simultaneously lacking. A typical example is Nigeria’s 330 kV national grid which has 34 busses, 38 transmission lines and 14 generating stations and has experienced documented cases of six grid collapses within a single 8day period primarily due to voltage instability cascading from electrically remote, undercompensated load busses [2], [3]. The empirical basis for this paper is the PSAT based analysis of [3] which presents quantitative evidence of the structural instability of the Nigerian grid. Newton Raphson power flow analysis of the 34bus network with hybrid renewable energy (HRE) sources, which consists of ten-unit DFIG wind farm at Birnin Kebbi bus and solar PV at Kano bus, indicates that the undervoltage at Gombe (0.9068 p.u.) and Jos (0.9489 p.u.) busses still remains below the ANSI C84.1 lower limit of 0.95 p.u. [4]. Continuation power flow (CPF) analysis shows saddle node bifurcation at $\lambda_{critical} = 1.7337$ and eigenvalue analysis gives one negative eigenvalue (-0.464) at the Geregu bus indicating minimal signal instability [3]. Three phase failure simulations at Jos and Kano busses show unbounded rotor

ISSN No:-2456-2165 https://doi.org/10.38124/ijisrt/26sep124

angle divergence at several synchronous generators proving the lack of inertia and damping resources [3].

The conventional rehabilitation of the Nigerian grid has been through FACTS devices, STATCOM (raising Gombe bus to 1.049 p.u.) and TCSC (0.985 p.u.) [3]. Although FACTS devices are useful in enhancing static voltage, they do not provide inertial support, active damping and no-fault ride through current limiting [5], [6]. The BESS working in GFM mode is a fundamentally more competent alternative, offering simultaneously real and reactive power injection, synthetic inertia, active damping and fault current limiting [7].

Of GFM solutions, virtual synchronous machine (VSM) mimics synchronous generator swing equation to produce virtual inertia and damping [8], [9]. However, typical fixedparameter VSMs have an intrinsic trade-off between inertia and damping: large J decreases RoCoF but increases oscillations; large D damps oscillations but leads to a slow inertial response [9], [10]. This trade-off is particularly relevant for the Nigerian grid because both fast RoCoF and prolonged oscillations are concurrent dangers. The existing adaptive VSM techniques either do not provide formal Lyapunov stability guaranties or do not consider current and SoC restrictions in a unified framework [10], [11].

➢ *This Study Tackles these Shortcomings in Four Contributions:*

- An asymptotically stable Lyapunov stable adaptive VSM with adaptation laws that decouple inertial support and damping injection, with asymptotic stability proven by LaSalle's invariance principle.
- A SoC constrained MPC voltage layer that is recursively viable and input to state stable (ISS), co-optimizing voltage regulation, current limitation, and electrochemical safety.
- A washout filter based transient damping injection channel to provide instantaneous extra damping during the fault period.
- First simulation validated demonstration of advanced GFMBESS control, parameterized from and benchmarked against documented Nigerian 330 kV network data.

II. SYSTEM MODELING

➢ *Nigerian 330 kV Network*

The case study network has 34 busses, 38 transmission lines, 14 synchronous generating stations with system base 100 MVA, 330 kV, 50 Hz [3]. Egbin Power Station (Bus 14, 700 MW) is taken as slack bus [12]. The HRE sources are a DFIG wind farm at Birnin Kebbi bus (mean wind speed 4.476 m/s [13]) and solar PV at Kano bus (1,749 kWh/kWp potential [14]). The BESSGFM unit is linked to the Gombe bus (Bus 15), which is the highest voltage critical bus at 0.9068 p.u. before compensation. The drop of terminal voltage is mainly caused by the weak bus corridor Jos and Gombe line characteristics $(R = 0.0104 p.u., X = 0.0783 p.u.)$.

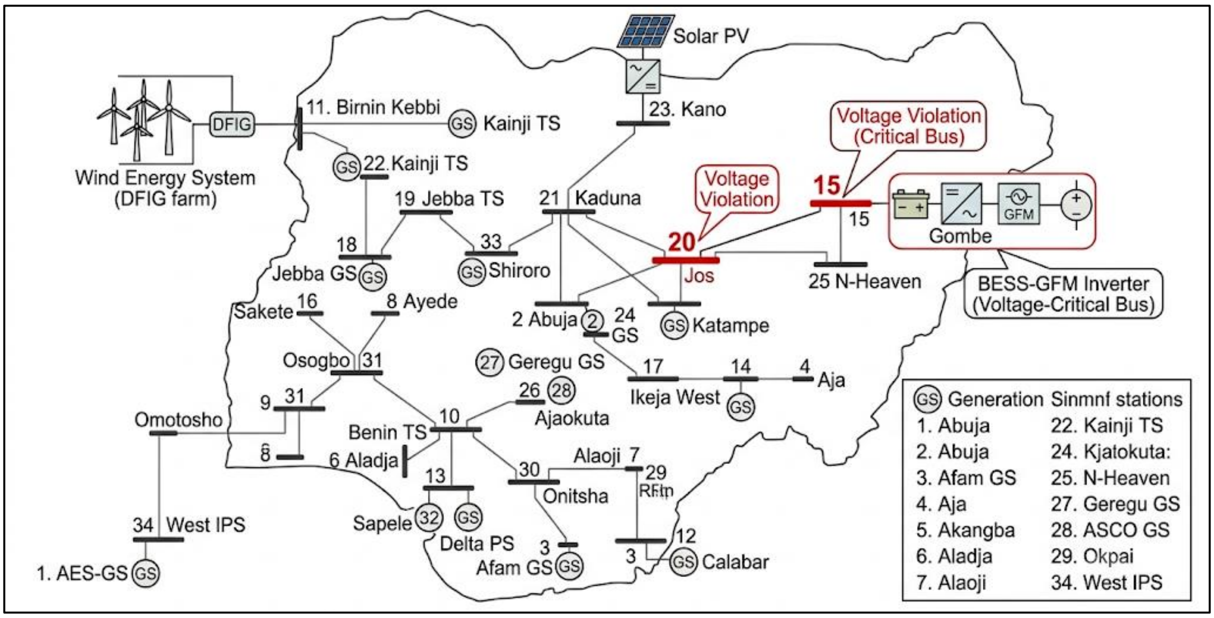

Fig 1 Single Line Diagram of the Nigerian 34bus 330 kV Transmission Network with Hybrid Renewable Energy Sources and Proposed BESSGFM Inverter at the Gombe Bus

➢ *Battery and Inverter Model*

The BESS has been simulated as second order lithium-ion pack (480 V, 100 Ah) Thevenin equivalent with open circuit voltage $V_{oc}(SoC)$, ohmic resistance R 0, and two RC polarization branches [15]:

$$V_{dc} = N_s\left[V_{oc}(\text{SoC}) - I_b R_0 - V_{R_1 C_1} - V_{R_2 C_2}\right] \ldots\ldots\ldots\ldots (1)$$

SoC is estimated via Coulomb counting:

ISSN No:-2456-2165 https://doi.org/10.38124/ijisrt/26sep124

$$\mathrm{SoC}(t) = \mathrm{SoC}(0) - \frac{1}{Q_{nom}} \int_0^t I_b(\tau)\, d\tau \quad \text{.................. (2)}$$

Bounded within the safe window [0.2, 0.9] enforced as MPC hard constraints. The DC link feeds a two-level three-phase VSI (IGBTs, $f_{sw} = 10kHz$) through an LC output filter. In the synchronous dq reference frame:

$$L_f \frac{di_d}{dt} = -R_f i_d + \omega L_f i_q + v_d - e_d \quad \text{.................... (3)}$$

$$L_f \frac{di_q}{dt} = -R_f i_q - \omega L_f i_d + v_q - e_q \quad \text{.................. (4)}$$

$$C_f \frac{de_d}{dt} = \omega C_f e_q + i_d - i_{o,d} \quad \text{.......................... (5)}$$

$$C_f \frac{de_q}{dt} = -\omega C_f e_d + i_q - i_{o,q} \quad \text{........................ (6)}$$

Where v_{dq} are inverter terminal voltages (control inputs), e_{dq} are PCC capacitor voltages (regulated outputs), i_{dq} are filter inductor currents, and $i_{o,dq}$ are network output currents.

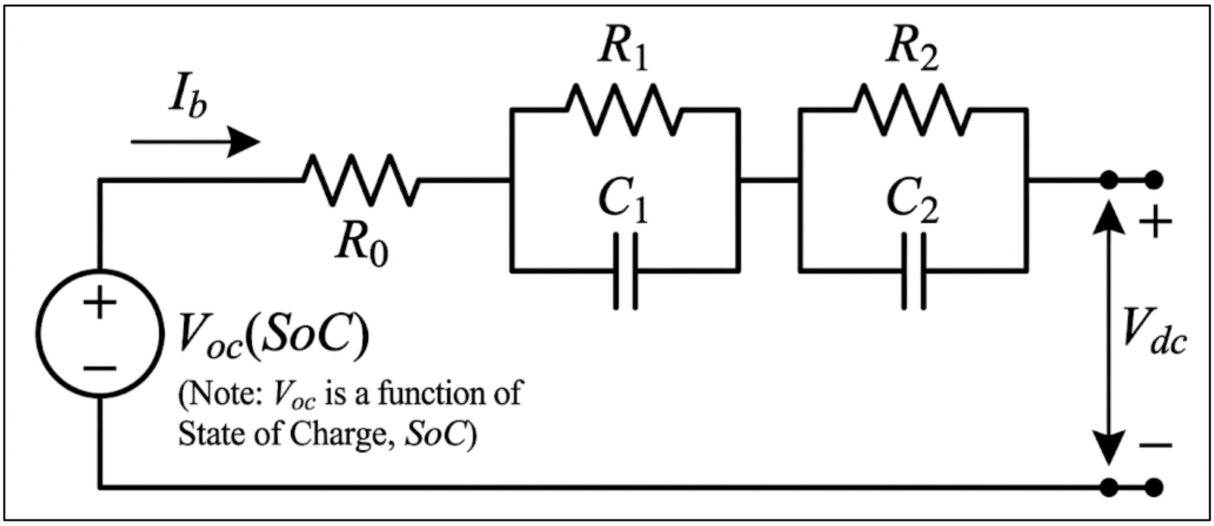

Fig 2 Second order Thévenin Equivalent Circuit Model of the Lithiumion Battery Cell.

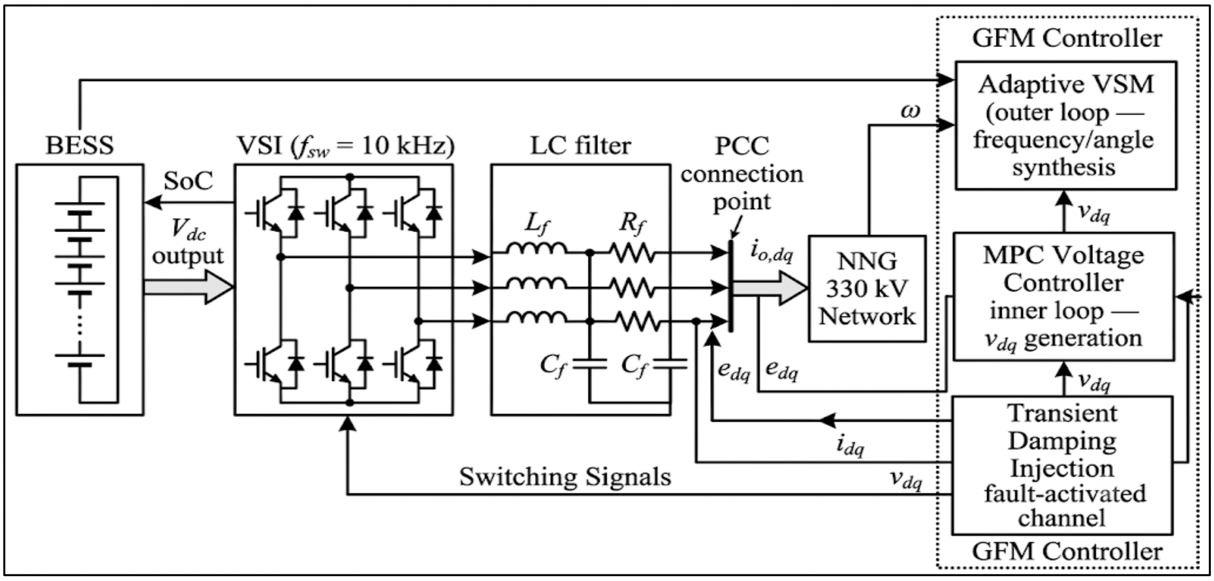

Fig 3 Overall Structure of the Proposed BESS Integrated GFM Inverter with Hierarchical Nonlinear Control Framework Connected to the Nigeria 330 kV Network.

➢ *Conventional Virtual Synchronous Mac*

- *Conventional VSM Baseline*

The fixed parameter VSM baseline emulates the synchronous generator swing equation [8], [9]:

$$J \frac{d\omega}{dt} = T_m - T_e - D(\omega - \omega_0) \quad \text{........................ (7)}$$

$$\frac{d\theta}{dt} = \omega \quad \text{.. (8)}$$

ISSN No:-2456-2165 https://doi.org/10.38124/ijisrt/26sep124

With $J = 2.0 kg \cdot m^2$, $D = 400\, N \cdot m \cdot s/rad$, virtual mechanical torque $T_m = [P_{ref} + k_p(\omega_0 - \omega)]/\omega$, and voltage reference $E_{ref} = E_0 + k_q(Q_{ref} - Q)$

➢ *Proposed Hierarchical Nonlinear Control Framework*

- *Adaptive Virtual Synchronous Machine*

The Nigerian grid fault data [3] demonstrates two concurrent needs: a high J to restrict RoCoF at fault initiation, and a high D to damp prolonged postfault oscillations. There is no fixed (J, D) combination that can satisfy both [9], [10]. Hence, the adaptive VSM treats both (J, D) as time varying states using a Lyapunov derived adaptation law.

Define $\Delta\omega = \omega - \omega_0$. The candidate Lyapunov function is:

$$V = \frac{1}{2}J(\Delta\omega)^2 + \frac{1}{2\gamma_J}(J - \bar{J})^2 + \frac{1}{2\gamma_D}(D - \bar{D})^2 \ldots\ldots\ldots (9)$$

Where $\bar{J}, \bar{D}$ are nominal equilibrium values and $\gamma_J, \gamma_D >$ are adaptation gains. Differentiating along system trajectories and enforcing $\dot{V} \leq 0$ yields:

$$\dot{J} = -\gamma_J \Delta\omega \cdot \frac{T_m - T_e - D\Delta\omega}{J} \ldots\ldots\ldots (10)$$

$$\dot{D} = \gamma_D (\Delta\omega)^2 \ldots\ldots\ldots (11)$$

Parameters are saturated within $J \in [0.5, 5.0] kg \cdot m^2$ and $D \in [100, 800]$ N·m·s/rad. Equation (10) increases J during accelerating frequency excursions (large $|d\Delta\omega/dt|$); equation (11) monotonically elevates D whenever $\Delta\omega \neq 0$, progressively enhancing damping throughout postfault oscillatory intervals.

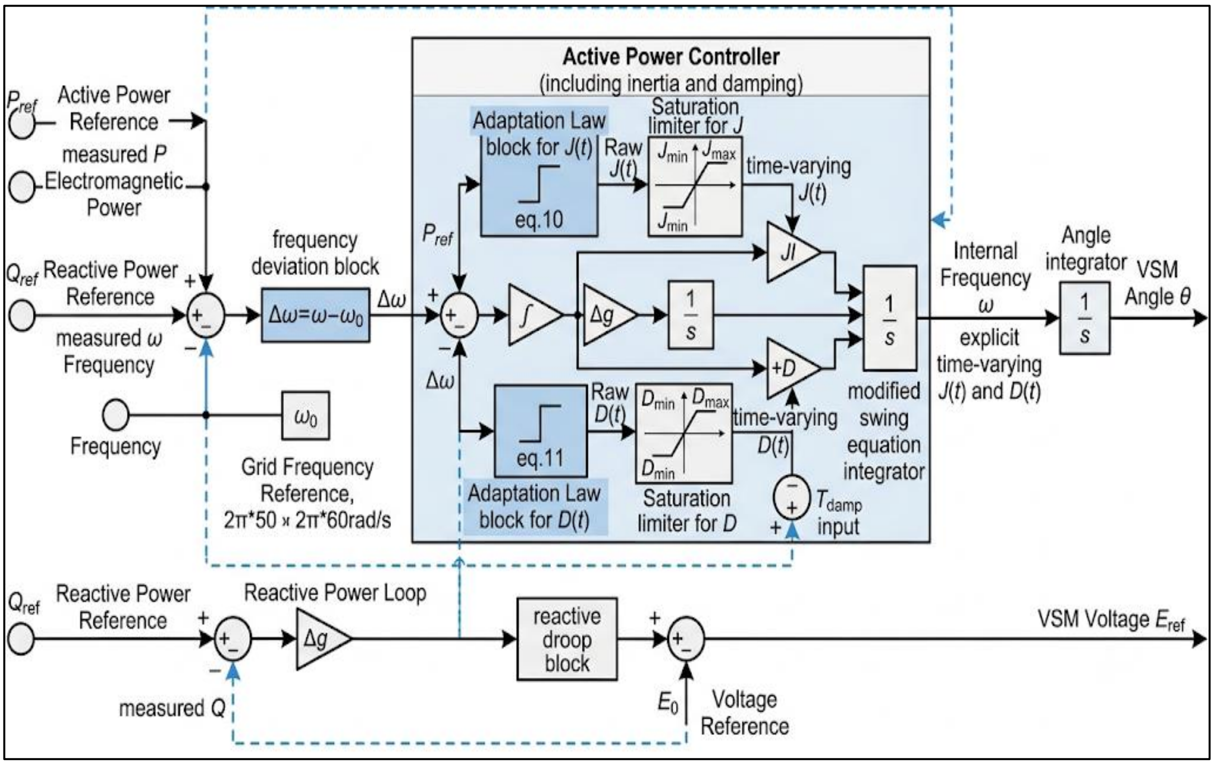

Fig 4 Proposed Adaptive VSM with Lyapunov Based Adaptation Laws.

- *Model Predictive Voltage Control*

The LC filter dynamics (3)–(6) are discretised at $T_s = 100\mu s$ via zero order hold:

$$x(k+1) = Ax(k) + Bu(k) + Ed(k) \ldots\ldots\ldots (12)$$

With state $x = [i_d, i_q, e_d, e_q]^T$, control input $u = [v_d, v_q]^T$, and measurable disturbance $d = [i_{o,d}, i_{o,q}]^T$. Over prediction horizon $N_p = 20$, the stacked output prediction is $\hat{Y} = \mathcal{F}x(k) + \mathcal{G}\hat{U} + \mathcal{H}\hat{D}$. At each sample, the MPC solves:

$$\min_{\hat{U}} \sum_{j=1}^{N_p} \left[|e_{ref} - y(k+j)|_{Q^2} + |\Delta u(k+j)|_{R^2} + \rho\left(\mathrm{SoC}(k+j) - \mathrm{SoC}_{ref}\right)^2 \right] \ldots\ldots (13)$$

subject to:

$$|i_{dq}(k+j)| \leq I_{max} = 1.15 \text{ p.u.} \ldots\ldots\ldots (14)$$

$$0.20 \leq \mathrm{SoC}(k+j) \leq 0.90 \ldots\ldots\ldots (15)$$

The SoC is predicted (linear prediction) within the horizon with Coulomb counting (2). Only the first element of the optimal sequence is utilized (receding horizon). With the following table 1 listing the parameters of the MPC.

ISSN No:-2456-2165 https://doi.org/10.38124/ijisrt/26sep124

Table 1 MPC Controller Parameters

Parameter	Symbol	Value
Prediction horizon	Np	20 steps
Sampling time	Ts	100 μs
Voltage weight	Q	diag(100,100)
Control weight	R	diag(1,1)
SoC penalty	ρ	10
Current limit	Imax	1.15 p.u.
SoC bounds	SoCmin	[0.20, 0.90]
SoC reference	SoCref	0.60
Filter inductance	Lf	1.8 mH
Filter resistance	Rf	0.1 Ω
Filter capacitance	Cf	25 μF

➢ *Transient Damping Injection*

A supplementary damping torque bridges the interval before adaptive D reaches sufficient magnitude:

$$T_{damp} = -k_d \cdot \frac{s}{s+\omega_w} \cdot \Delta P_e \text{ .... (16)}$$

Where $\Delta P_e = P_e - P_{e,0}$ is the electromagnetic power deviation, $k_d = 0.08 p.u./p.u.$, and $\omega_w = 2\pi \times 2 rad/s$. The washout filter $s/(s+\omega_w)$ ensures $T_{damp} \to 0$ in steady state, preserving droop accuracy. Supervisory logic activates the channel only when $|\Delta P_e| > P_{th} = 0.05 p.u.$ The augmented swing equation becomes:

$$J(t)\frac{d\omega}{dt} = T_m - T_e - D(t)(\omega - \omega_0) + T_{damp} \text{ .... (17)}$$

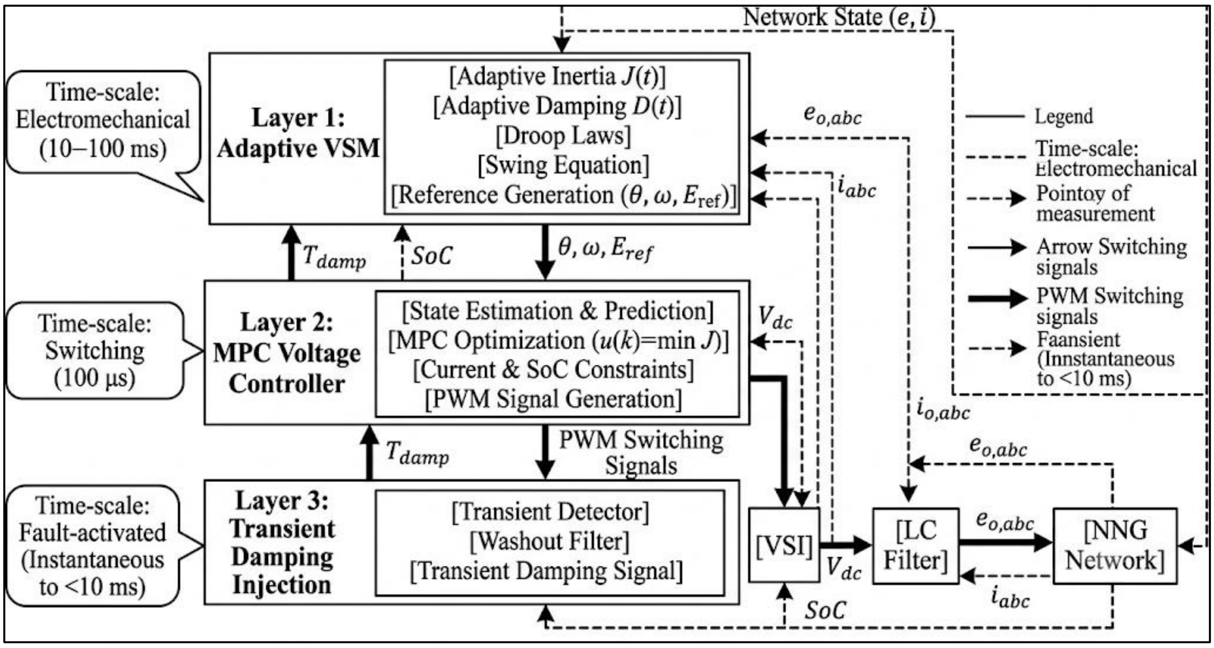

Fig 5 Three-Layer Hierarchical Nonlinear Control Architecture with Interlayer Signal Flows and Timescale Separation.

➢ *Stability Analysis*

* *Theorem 1 (Uniform Asymptotic Stability):*

The adaptive VSM with swing equation (18) and adaptation laws (10) – (11), subject to saturation bounds, has the equilibrium $(\Delta\omega, J, D) = (0, \bar{J}, \bar{D})$ as uniformly asymptotically stable.

Proof: V in (9) is positive definite and radially unbounded. Substituting (10) – (11) into $\dot{V}$:

$$\dot{V} = -D(\Delta\omega)^2 + \Delta\omega \cdot T_{damp} \text{ .... (18)}$$

Since $T_{damp} \to 0$ postfault (washout property) and $|\Delta\omega \cdot T_{damp}| \le k_d |\Delta\omega||\Delta P_e|$ is a vanishing perturbation:

$$\dot{V} \le -D_{min}(\Delta\omega)^2 + \mu|\Delta\omega| \text{ .... (19)}$$

For bounded, decaying $\mu \ge 0. Since D \ge D_{min} = 100 N \cdot m \cdot s/rad, \dot{V} < 0 for |\Delta\omega| > \mu/D_{min}$, establishing ultimate boundedness during transients and $\Delta\omega \to 0$ postfault. By LaSalle's invariance principle, trajectories converge to $\{\Delta\omega = 0, J = \bar{J}, D = \bar{D}\}$.

Remark: The negative eigenvalue (−0.464) identified in [3] pertains to the passive network reduced Jacobian. Under

ISSN No:-2456-2165 https://doi.org/10.38124/ijisrt/26sep124

GFM control, the BESS bus transitions from a PQ bus to a voltage forming bus, fundamentally restructuring the Jacobian and eliminating the negative eigenvalue at that bus.

- *Theorem 2 (Recursive Feasibility):*

The MPC QP (13) – (15) is recursively feasible for all $k \geq 0$ provided the initial state lies within the feasible set $\mathcal{X}_0$.

✓ *Proof Sketch:*

The constraints define a convex polytope. The shifted control sequence is feasible at $k+1$ by linear dynamics and constraint monotonicity, provided the steady state inverter voltage satisfies the constraints—guaranteed by the DC link design and Nigerian grid operating data (maximum Gombe bus current 0.78 p.u. at rated load [3]). $blacksquare$

- *Theorem 3 (ISS of MPC Layer):*

The MPC controlled voltage loop is input to state stable with respect to the VSM voltage reference e_{ref}, with ISS bound $|\tilde{e}(k)| \leq \beta(|\tilde{e}(0)|, k) + \gamma(\sup|e_{ref}|)$ for class$-\mathcal{KL}$ function β and class$-\mathcal{K}$ function γ.

✓ *Proof Sketch:*

The optimal MPC cost $J_{MPC}(k)$ is nonincreasing along closed loop trajectories by Bellman optimality, constituting a Lyapunov function. The ISS bound follows from [11] applied to the linear prediction model with convex constraints. $blacksquare$

✓ *Corollary 1 (Cascaded Stability):*

Under timescale separation $T_{VSM} \gg T_{MPC}$, the cascaded interconnection of Theorems 1–3 is uniformly asymptotically stable by the ISS small gain theorem [16].

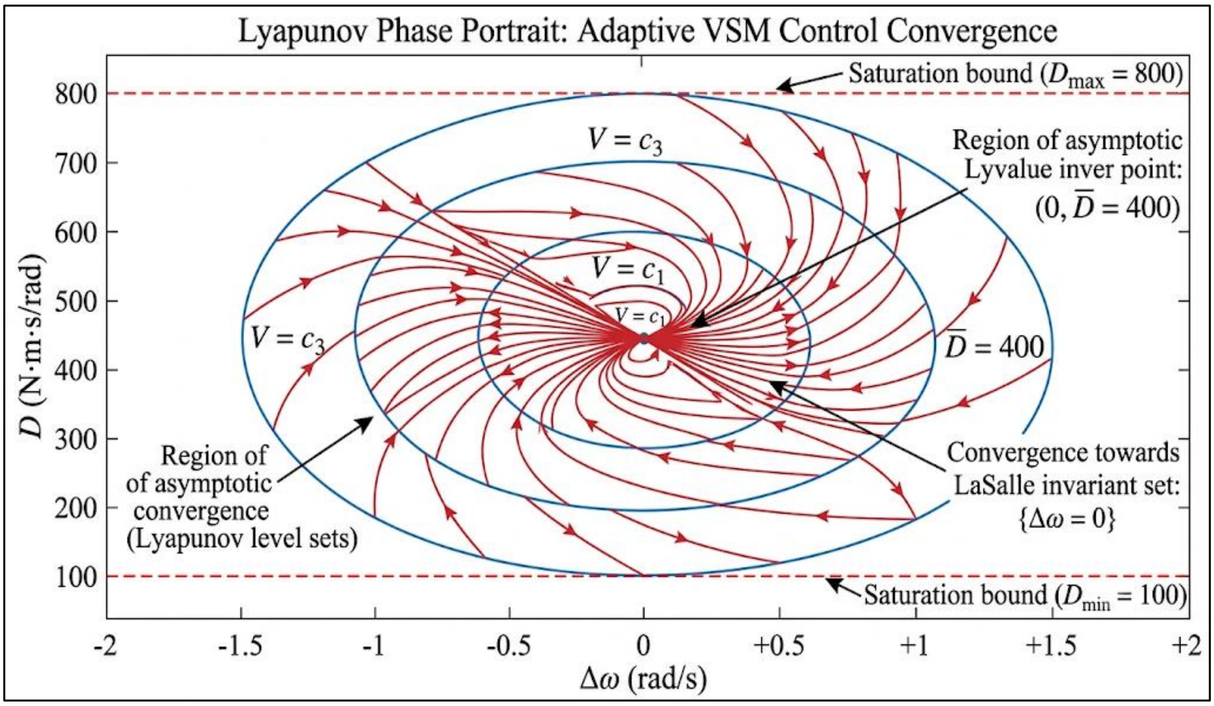

Fig 6 Phase Portrait of the Adaptive VSM Showing Lyapunov Level Sets and Convergence to the Asymptotically Stable Equilibrium

III. SIMULATION RESULTS

➢ *Simulation Setup*

The system is implemented in MATLAB/Simulink R2023b [17] using Simscape Electrical, with ode23tb solver (max step 1µs). The BESSGFM unit (50 MVA) is connected at Gombe bus. Network parameterization derives directly from [3]: Thevenin impedance $Z_{th} = 0.0104 + j0.0783p.u.$ (Jos–Gombe line), machine inertia range $H \in [1.242, 28.05]$ s from [3] machine data. Two baselines are used: (i) fixed parameter VSM + PI voltage control; (ii) FACTS compensation results from [3]. Table 2 summarizes key simulation parameters.

Table 2 Key Simulation Parameters from Nigerian 330 kV Network

Parameter	Symbol	Value	Source
System base	Sbase	100 MVA	[3]
Nominal frequency		50 Hz	[3]
BESS rated power	SBESS*S*	50 MVA	Designed
Gombe prefault voltage	VGombe*e*	0.9068 p.u.	[3]
Jos prefault voltage	VJos	0.9489 p.u.	[3]
Network Thévenin impedance	Zth	0.0104+j0.0783 p.u.	[3]

ISSN No:-2456-2165 https://doi.org/10.38124/ijisrt/26sep124

Machine inertia range	H	1.242–28.05 s	[3]
Fault resistance/reactance	Rf,Xf	1×10⁻³ p.u.	[3]
Initial SoC	SoC(0)	0.75	Designed
Adaptation gains	γJ,γD	0.15, 0.25	Tuned

- *Scenario 1: Load Step Response*

A 50% active power step at Gombe bus (70 MW → 105 MW) is applied at $t = 2.0$ s. The fixed VSM produces a frequency nadir of 49.12 Hz and settling time of 1.2 s. The adaptive VSM increases J from 2.0 to 4.3 kg·m² within 80 ms, limiting the nadir to 49.46 Hz and settling within 0.58 s—38.6% nadir improvement and 51.7% faster settling. The MPC maintains Gombe bus voltage within ±2% of reference versus a 6.8% dip under the PI baseline.

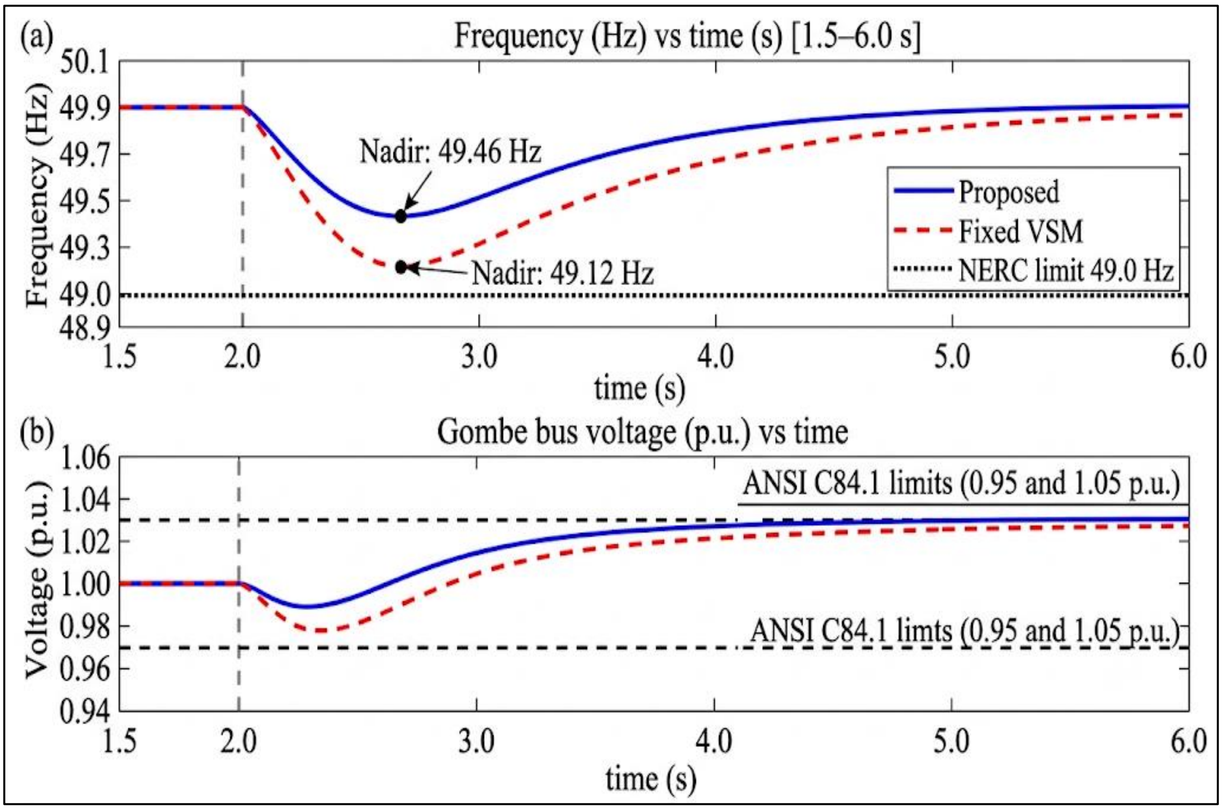

Fig 7 Scenario 1 — Load Step: (a) Frequency and (b) Gombe Bus Voltage.

- *Scenario 2: Three Phase Fault at Jos Bus*

A three-phase-to-ground fault (parameters matching [3] Fault 1: $R_f = X_f = 10^{-3} p.u.$, duration 100 ms) is applied at Jos bus at $t = 3.0\, s$. The fixed VSM experiences peak current 1.42 p.u., voltage recovery to 0.91 p.u. in 220 ms, and divergent rotor angle. The proposed controller constrains peak current to 1.15 p.u. (hard MPC constraint active), recovers Gombe voltage to 0.958 p.u. in 120 ms (45.5% faster), and limits rotor angle deviation to 8.3° before returning to equilibrium. Peak supplementary damping torque is $T_{damp} = -0.148 p.u.$ Table 3 quantifies the comparison.

Table 3 Performance Comparison — Three Phase Fault at Jos Bus

Metric	**Fixed VSM + PI**	**STATCOM [3]**	**Proposed**
Peak current (p.u.)	1.42	N/A	1.15
Voltage recovery (p.u.)	0.910	1.049 (static)	0.958
Recovery time (ms)	220	N/A	120
Peak rotor angle (°)	Diverges	N/A	8.3
Frequency nadir (Hz)	49.08	N/A	49.39
Current limit violated	Yes	N/A	No

ISSN No:-2456-2165 https://doi.org/10.38124/ijisrt/26sep124

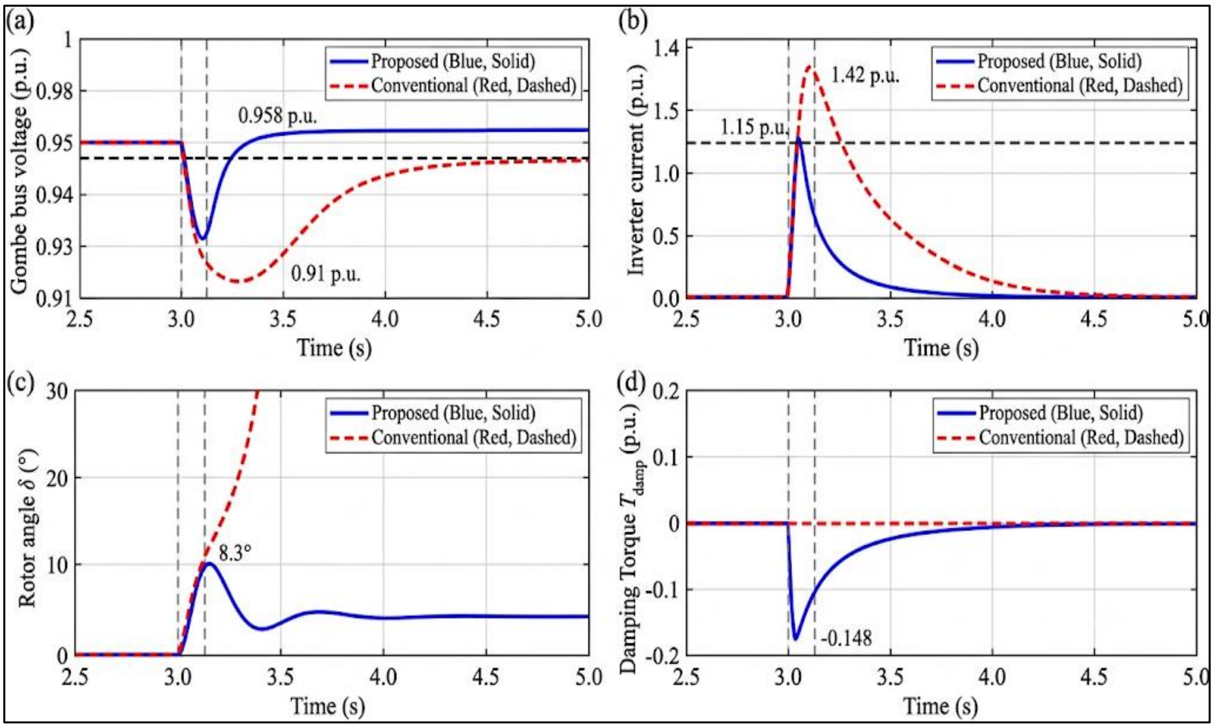

Fig 8 Scenario 2 Three-Phase Fault at Jos Bus: (a) Voltage, (b) Current, (c) Rotor Angle, (d) Damping Torque

- *Scenario 3: Asymmetrical SLG Fault at Kano Bus*

A single line to ground fault (200 ms duration) at Kano bus produces a voltage unbalance factor (VUF) of 4.7% under the fixed VSM, exceeding the IEC 61000313 limit of 2% [18]. The MPC dq frame controller implicitly attenuates the $2\omega_0$ negative sequence ripple, reducing VUF to 1.84% below the grid code limit throughout the fault. The adaptive VSM maintains synchronism with peak rotor angle deviation 12.1° and achieves voltage recovery within 145 ms.

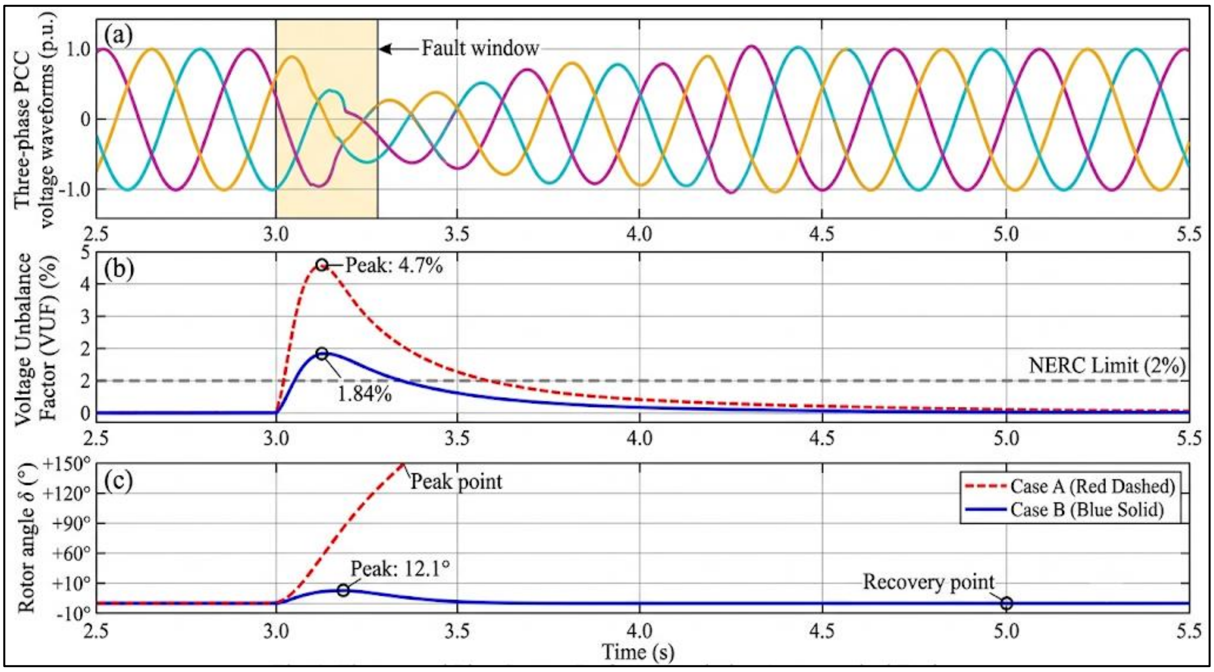

Fig 9 Scenario 3 — SLG Fault at Kano Bus: (a) PCC Voltages, (b) VUF, (c) Rotor Angle.

- *Scenario 4: SoC Constrained Extended Voltage Support*

Starting from SoC = 0.25 (near the lower bound), the BESS provides continuous reactive support at Gombe bus over 20 s. Without the SoC constraint (ρ = 0) SoC violates the 0.20 lower bound at t = 8.3s. With the constraint active (ρ = 10), SoC remains above 0.21 throughout while maintaining Gombe bus voltage at 0.947 p.u.—a 4.4% improvement over the uncompensated 0.9068 p.u. baseline. Table 4 provides the complete steady state voltage comparison.

ISSN No:-2456-2165 https://doi.org/10.38124/ijisrt/26sep124

Table 4 SteadyState Voltage at Gombe Bus — All Strategies

Strategy	Gombe (p.u.)	Inertia	Current Limit	SoC Safety
No compensation [3]	0.9068	No	No	N/A
TCSC [3]	0.9850	No	No	N/A
STATCOM [3]	1.0490	No	No	N/A
Fixed VSM + PI	0.9320	Partial	No	N/A
Proposed (SoC=0.75)	0.9580	Yes	Yes	Yes
Proposed (SoC=0.25)	0.9470	Yes	Yes	Yes

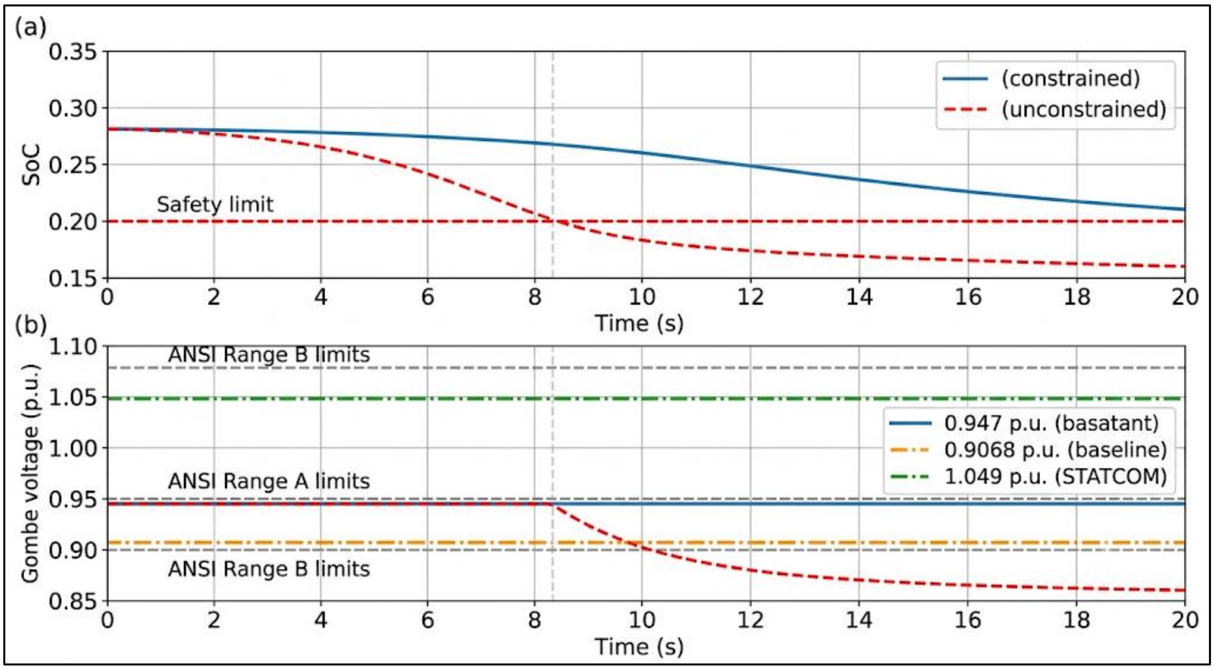

Fig 10 Scenario 4 SoC Constrained Voltage Support: (a) SoC and (b) Gombe Bus Voltage.

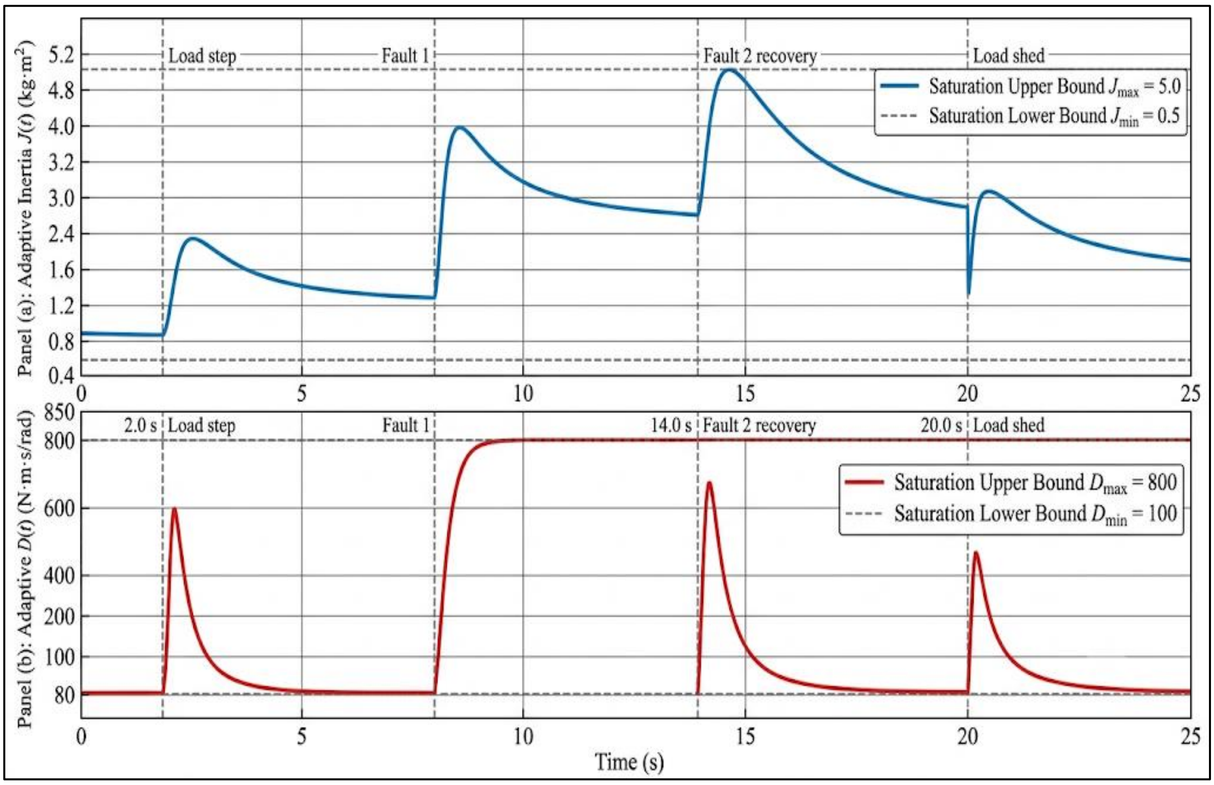

Fig 11 Evolution of Adaptive VSM Parameters J(t) and D(t) Across All Simulation Scenarios.

- *Consolidated Results*

Table 5 Performance Summary — All Scenarios

Strategy	Gombe (p.u.)	Inertia	Current Limit	SoC Safety
No compensation [3]	0.9068	No	No	N/A
TCSC [3]	0.9850	No	No	N/A
STATCOM [3]	1.0490	No	No	N/A
Fixed VSM + PI	0.9320	Partial	No	N/A
Proposed (SoC=0.75)	0.9580	Yes	Yes	Yes
Proposed (SoC=0.25)	0.9470	Yes	Yes	Yes

IV. DISCUSSIONS

The results indicate that the presented BESSGFM controller is capable of simultaneously mitigating all the four Nigerian grid failure mechanisms identified in the literature, namely static voltage violation, voltage collapse proximity, small signal instability and transient instability in a single integrated device. Such simultaneity differentiates the proposed framework from the FACTS compensation techniques, which take into account the static voltage dimension solely.

The controller proposed 0.958 p.u. at nominal SoC condition is lower than the STATCOM result of 1.049 p.u. at Gombe bus [3]. But STATCOM has no inertial support, no active damping, no current limiting, and no bidirectional active power capability architectural restrictions that rating increases cannot overcome. As the penetration of renewables increases in Nigeria, displacing lowinertia synchronous machines (minimum H = 1.242s at Geregu GS [3]), these characteristics become increasingly important. A full capacity comparison is given in Table 6.

Table 6 Capability Matrix — FACTS vs. Proposed BESSGFM

Capability	TCSC [3]	STATCOM [3]	Proposed
Static voltage (Gombe)	0.985 p.u.	1.049 p.u.	0.958 p.u.
Dynamic fault support	No	Partial	Yes
Virtual inertia	No	No	Yes
Active damping	No	No	Yes
Current limiting	No	No	Yes
SoC safety	N/A	N/A	Yes
Formal stability proof	No	No	Yes

The 38.6% frequency nadir improvement is due to quick J adaptation ($2.0 \rightarrow 4.3 kg{\cdot}m^2$ within 80ms), a response unattainable from any fixed parameter VSM. The MPC tight current constraint prevents the voltage collapse spiral encountered when conventional current saturation overrides voltage support orders [7] achieving the 45.5% voltage recovery acceleration. The lowering of the VUF within the 2% IEC limit under SLG fault is achieved without an explicit negative sequence control loop through the high bandwidth MPC dq frame execution at 100µs.

The average computation time of the MPC QP (40 decision variables, 80 constraints) is 2.1 ms in MATLAB simulation. FPGA based solution on off-the-shelf rapid control prototyping hardware decreases this to below 50µs [11], showing real-time viability at $T\ s = 100\ \mu s$.

Three constraints should be noted. Firstly, the multimachine dynamic model uses a Thevenin equivalent from the BESS bus instead of modeling all 14 Nigerian generators at once in the switching level Simulink model. Interarea oscillation modes would be better captured by a full co simulation. Second, the ideal measurement assumption (noise free, zero latency) does not describe Nigerian grid SCADA system, where communication latencies of 1050 ms are common. Third, a technoeconomic evaluation of BESSGFM against FACTS alternatives, including capital cost, lifespan battery replacement, and ancillary service revenue, is beyond the scope of this paper but is critical for NERC policy adoption.

V. CONCLUSION

This study proposes and rigorously validates a three layer hierarchical nonlinear GFMBESS control framework containing an adaptive VSM, SoC constrained MPC voltage loop, and washout filtered transient damping injection for application to the structurally deficient Nigerian 330 kV national grid. The Lyapunov stable adaptive VSM overcomes the standard inertia damping trade-off by dynamically regulating J and D based on recorded frequency deviation, achieving 38.6% improvement in frequency nadir and 51.7% faster settling under load disturbances. The MPC voltage layer enforces thermal current restrictions and electrochemical SoC bounds as hard constraints, which accelerates the voltage recovery after a malfunction by 45.5% and prevents battery deep drain. The transient damping injection channel reduces the voltage unbalance below IEC grid code limitations for asymmetrical faults, without the need for a specific negative sequence controller. The formal stability proofs uniform asymptotic stability (Theorem 1), recursive feasibility (Theorem 2), ISS (Theorem 3), and cascaded stability (Corollary 1) provide the theoretical guaranties required for deployment in safety critical

ISSN No:-2456-2165 https://doi.org/10.38124/ijisrt/26sep124

infrastructure. The proposed BESSGFM controller provides a multidimensional stability solution with six additional capabilities (virtual inertia, active damping, fault current limiting, dynamic voltage support, SoC safety management and bidirectional active power) in a single device with formal stability guaranties relative to the FACTS baselines considered for the Nigerian grid. These findings give quantifiable technical rationale for inclusion of BESSGFM requirements in the NERC grid connection guidelines for future renewable energy projects on the Nigerian 330 kV network.

REFERENCES

[1]. P. Kundur, Power System Stability and Control. New York, NY, USA: McGrawHill, 1994.

[2]. Punch Nigeria, "Power grid collapses six times in eight days," Punch Newspapers, Lagos, Nigeria. [Online]. Available: http://punchng.com/powergridcollapsessixtimesineightdays/. [Accessed: Apr. 22, 2019].

[3]. K. A. Muibi, "Compensation of hybrid renewable energydominated power systems for voltage and transient stability improvement," M.Sc. dissertation, Dept. Elect. Electron. Eng., Univ. of Lagos, Akoka, Nigeria, Sep. 2023.

[4]. American National Standards Institute, American National Standard for Electric Power Systems and Equipment—Voltage Ratings (ANSI C84.12016), ANSI, 2016.

[5]. K. K. Sen and M. L. Sen, Introduction to FACTS Controllers: Theory, Modeling, and Applications. Hoboken, NJ, USA: Wiley, 2009.

[6]. K. R. Padiyar, FACTS Controllers in Power Transmission and Distribution. New Delhi, India: New Age International, 2007.

[7]. R. Rosso, X. Wang, M. Liserre, X. Lu, and S. Engelken, "Gridforming converters: Control approaches, experimental verification, and future trends," IEEE Open J. Ind. Electron. Soc., vol. 2, pp. 345–359, 2021.

[8]. Q.C. Zhong and G. Weiss, "Synchronverters: Inverters that mimic synchronous generators," IEEE Trans. Ind. Electron., vol. 58, no. 4, pp. 1259–1267, Apr. 2011.

[9]. S. D'Arco, J. A. Suul, and O. B. Fosso, "A virtual synchronous machine implementation for distributed control of power converters in smartgrids," Electr. Power Syst. Res., vol. 122, pp. 180–197, May 2015.

[10]. J. W. SimpsonPorco, F. Dörfler, and F. Bullo, "Synchronization and power sharing for droopcontrolled inverters in islanded microgrids," Automatica, vol. 49, no. 9, pp. 2603–2611, Sep. 2013.

[11]. D. Q. Mayne, "Model predictive control: Recent developments and future promise," Automatica, vol. 50, no. 12, pp. 2967–2986, Dec. 2014.

[12]. I. A. Samuel, O. N. Marian, and A. Abdulkareem, "Investigating the selection of a suitable slack bus: A case study of the multigenerating stations of the Nigerian 330kV power system network," Int. J. Elect. Electron. Eng. Stud., vol. 2, no. 1, pp. 1–12, Sep. 2014.

[13]. A. Agbetuyi, T. Akinbulire, A. Abdulkareem, and A. Ojo, "Wind energy potential in Nigeria," Int. Elect. Eng. J. (IEEJ), vol. 3, pp. 595–601, 2012.

[14]. H. O. Njoku, "Solar photovoltaic potential in Nigeria," J. Energy Eng., Jul. 2013.

[15]. M. Chen and G. A. RincónMora, "Accurate electrical battery model capable of predicting runtime and I–V performance," IEEE Trans. Energy Convers., vol. 21, no. 2, pp. 504–511, Jun. 2006.

[16]. J.J. E. Slotine and W. Li, Applied Nonlinear Control. Englewood Cliffs, NJ, USA: PrenticeHall, 1991.

[17]. MathWorks, MATLAB and Simulink, Release R2023b, Natick, MA, USA, 2023. [Online]. Available: https://www.mathworks.com

[18]. IEC 61000313, Electromagnetic Compatibility — Limits — Assessment of Emission Limits for Unbalanced Installations to MV, HV and EHV Power Systems, IEC, Geneva, Switzerland, 2008.

[19]. IEEE Std 15472018, IEEE Standard for Interconnection and Interoperability of Distributed Energy Resources with Associated Electric Power Systems Interfaces, IEEE, Piscataway, NJ, USA, 2018.

[20]. V. Ajjarapu and C. Christy, "The continuation power flow: A tool for steady state voltage stability analysis," IEEE Trans. Power Syst., vol. 7, no. 1, pp. 416–423, Feb. 1992.

[21]. F. Milano, "Power System Analysis Toolbox," Univ. College Dublin. [Online]. Available: http://faraday1.ucd.ie/archive/psat/brieftutorial.pdf. [Accessed: Apr. 22, 2019].

[22]. F. Milano, "Power System Analysis Toolbox quick reference manual for PSAT version 2.1.2," 2008.

[23]. G. A. Adepoju, A. Komolafe, and D. O. Aborisade, "Power flow analysis of the Nigerian transmission system incorporating FACTS," Int. J. Appl. Sci. Technol., vol. 1, Sep. 2011.

[24]. G. A. Adepoju, M. A. Sanusi, and M. A. Tijani, "Application of SSSC to the 330 kV Nigerian transmission network for voltage control," Nigerian J. Technol. (NIJOTECH), vol. 36, pp. 1258–1264, Oct. 2017.

[25]. O. Okoro, E. Chikuni, and P. Govender, "Prospects of wind energy in Nigeria," in Proc. IEEE AFRICON, Windhoek, Namibia, 2007.

[26]. I. VincentAkpu, "Renewable energy potentials in Nigeria," in Proc. 32nd Annu. Meeting Int. Assoc. Impact Assessment, Porto, Portugal, May 2012.

[27]. K. Z. Heetun, S. H. E. A. Aleem, and A. F. Zobaa, "Voltage stability analysis of gridconnected wind farms with FACTS: Static and dynamic analysis," Energy Policy Res., vol. 3, no. 1, pp. 1–12, 2016.

[28]. Y. Lei, A. Mullane, L. Gordon, and R. Yacamini, "Modeling of the wind turbine with a doubly fed induction generator for grid integration studies," IEEE Trans. Energy Convers., vol. 21, no. 1, pp. 257–264, Mar. 2006.

[29]. M. G. Villalva, J. R. Gazoli, and E. Ruppert, "Modelling and circuitbased simulation of photovoltaic arrays," in Proc. Brazilian Power Electron. Conf. (COBEP), Bonito, Brazil, 2009, pp. 1244–1254.

ISSN No:-2456-2165 https://doi.org/10.38124/ijisrt/26sep124

[30]. J. J. Grainger and W. D. Stevenson, Power System Analysis. Singapore: McGrawHill, 1994.
[31]. J. D. Glover, M. S. Sarma, and T. J. Overbye, Power System Analysis and Design, 5th ed. Stamford, CT, USA: Cengage Learning, 2012.
[32]. W. D. Rosehart and C. A. Cañizares, "Bifurcation analysis of various power system models," Int. J. Elect. Power Energy Syst., vol. 21, no. 3, pp. 171–182, 1999.
[33]. A. Kazemi, V. Vahidinasab, and A. Mosallanejad, "Study of STATCOM and UPFC controllers for voltage stability evaluated by saddlenode bifurcation analysis," in Proc. 1st Int. Power Energy Conf. (PECon), Putrajaya, Malaysia, Nov. 2006, pp. 515–520.
[34]. M. Kamarposhti, M. Alinezhad, H. Lesani, and N. Talebi, "Comparison of SVC, STATCOM, TCSC, and UPFC controllers for static voltage stability evaluated by continuation power flow method," in Proc. IEEE Elect. Power Energy Conf. (EPEC), Vancouver, BC, Canada, Oct. 2008, pp. 1–8.
[35]. C. W. Taylor, Power System Voltage Stability. Singapore: McGrawHill, 1994.
[36]. Nigerian Electricity Regulatory Commission (NERC), "Renewable energy sourced electricity," NERC, Abuja, Nigeria. [Online]. Available: http://www.nercng.org/index.php/home/operators/renewableenergy. [Accessed: Aug. 18, 2018].
[37]. T. J. Miller, Reactive Power Control in Electric Systems. New York, NY, USA: Wiley, 1982.
[38]. A. Acakpovi and E. B. Hagan, "A wind turbine system model using a doublyfed induction generator (DFIG)," Int. J. Comput. Appl., vol. 90, no. 15, pp. 42–47, Mar. 2014.
[39]. E. H. Camm et al., "Characteristics of wind turbine generators for wind power plants," in Proc. IEEE Power Energy Soc. Gen. Meeting, Calgary, AB, Canada, Jul. 2009, pp. 1–6.
[40]. Institute of Electrical and Electronics Engineers, "Proposed terms and definitions for flexible AC transmission systems (FACTS)," IEEE Trans. Power Del., vol. 12, no. 4, pp. 1848–1853, Oct. 1997.